Asociación Argentina
de Mecánica Computacional

Mecánica Computacional Vol XXXIV, págs. 2199-2215 (artículo completo)
Sebastián Giusti, Martín Pucheta y Mario Storti (Eds.)
Córdoba, 8-11 Noviembre 2016

VALIDATION OF A MULTISCALE MODEL OF THE SECOND SHUTDOWN SYSTEM OF AN EXPERIMENTAL NUCLEAR REACTOR

Ludmila M. Rechiman[1,2], **Mariano I. Cantero**[1,2,3], **Federico Caccia**[1,2] **and Enzo A. Dari**[1,2,3]

[1]*Departamento de Mecánica Computacional - Av. Bustillo 9500 Centro Atómico Bariloche, Comisión Nacional de Energía Atómica, http://www.mecom.cnea.gov.ar/*

[2]*Instituto Balseiro, Av. Bustillo 9500 Centro Atómico Bariloche, Universidad Nacional de Cuyo, http://www.ib.edu.ar/.*

[3]*CONICET - Consejo Nacional de Investigaciones Científicas y Técnicas, http://www.conicet.gov.ar*

Keywords: multiscale modeling, validation procedure, weak-coupling of dimensionally heterogeneous systems

Abstract. A three-dimensional multiscale numerical model is presented in order to describe the fluid dynamics associated to the Second Shutdown System (SSS) of an experimental nuclear reactor. Detailed computational fluid dynamics simulations were performed in a RA-10 SSS Mockup similar to the RA-10 SSS. The main component of the SSS is the reflector tank which must be drained in a limited amount of time through a series of pipes. The modeling of the complete system is based on coupling subsystems through dynamic boundary conditions. Numerical simulations results allow to determine the location of the free-surface in the tank. For validation purpose, the location of the interface was compared with experimental data measured in a local manner. For verification, the unsteady-state macroscopic mechanical energy balance was used. A good agreement between the several interface estimators after an initial transient with wave motion is shown. The results prove that the multiscale approach is suitable to reproduce the overall behavior of the fluid dynamics of RA-10 SSS Mockup.

1 INTRODUCTION

The RA-10 project is a new 30 MW_{th} multipurpose nuclear Research Reactor (RR) which will replace the RA-3 reactor. The main objective of this new reactor will be to provide radioisotopes for Latin America. This reactor is currently being designed and managed by the Argentinian National Atomic Energy Commision (CNEA) (Blaumann et al. (2013)).
The First Shutdown System (FSS) of the RA-10 reactor is based on the insertion of control rods. On the other hand, the Second Shutdown System (SSS) relies on removing the liquid reflector inside a tank surrounding the core through draining just due to the action of gravity. The SSS of this reactor is a class C safety system and its design is based on an equivalent system developed by INVAP for the Open Pool Australian Light-water reactor (OPAL)(Villarino and Doval (2011)).
The SSS is composed by subsystems with different characteristics. The only subsystem which requires a three-dimensional (3D) description is the one that involves the reflector tank. The remaining subsystems can be described by simple models. In this work a multiscale approach is employed to model the RA-10 SSS Mockup. The methodology involves coupling a 3D computational fluid dynamic (CFD) model of reflector tank subsystem with a zero-dimensional (0D) model of the other piping subsystems using dynamic boundary conditions.
In this article, the validation process of the numerical model of the RA-10 SSS Mockup and a performance analysis is presented. The analysis seeks to address in detail the fluid dynamics that takes place inside the reflector tank with the purpose of verifying if the safety criteria established for the SSS is accomplished.
The paper is organized as follows: Sec.(2) describes the main features of the RA-10 SSS. Sec.(3) describes the model of the discharge hydraulic net subsystem as well as the pressure equalization line subsystem. Sec.(4) presents an assessment of the solution based on unsteady-state macroscopic mechanical energy balance. Sec.(5) reports the results of the simple model applied to the Mockup facility. In Sec.(6) the full 3D-0D coupled model is detailed, while Sec.(7) presents the most relevant validation results of the full numerical model applied to the RA-10 SSS Mockup geometry. Finally Sec.(8) sums up the conclusions.

2 GENERAL DESCRIPTION OF SSS OF RA-10 REACTOR

The RA-10 SSS is mainly composed by three connected subsystems: the reflector tank, the discharge hydraulic net and the pressure equalization line. A simple diagram is shown in Fig.(1). When the SSS is required to act, a manifold of six valves located in the discharge hydraulic net will open and the fluid will start to drain by means of the body force associated to gravity. The liquid will flow from the reflector tank through the discharge net to a storage tank located below the core level. In order to have equal pressure at the storage tank and over the top of the reflector tank, a pressure equalization line is used. The reflector liquid is heavy water, and is covered by helium to preserve its purity.
The cover gas fills up the storage tank, the pressure equalization line and part of the expansion tank. During the performance of the SSS, the cover gas will enter through a connection located in the upper part of the reflector tank which is partially filled with liquid at the beginning of the evolution.
The overall dynamics of the SSS is accomplished by connecting the piping subsystems to the CFD model through corresponding dynamically changing boundary conditions.
Particularly, the discharge hydraulic net impose a pressure condition on the outflow of the reflector tank when the SSS is acting. Moreover, the equalization pressure line impose a pressure

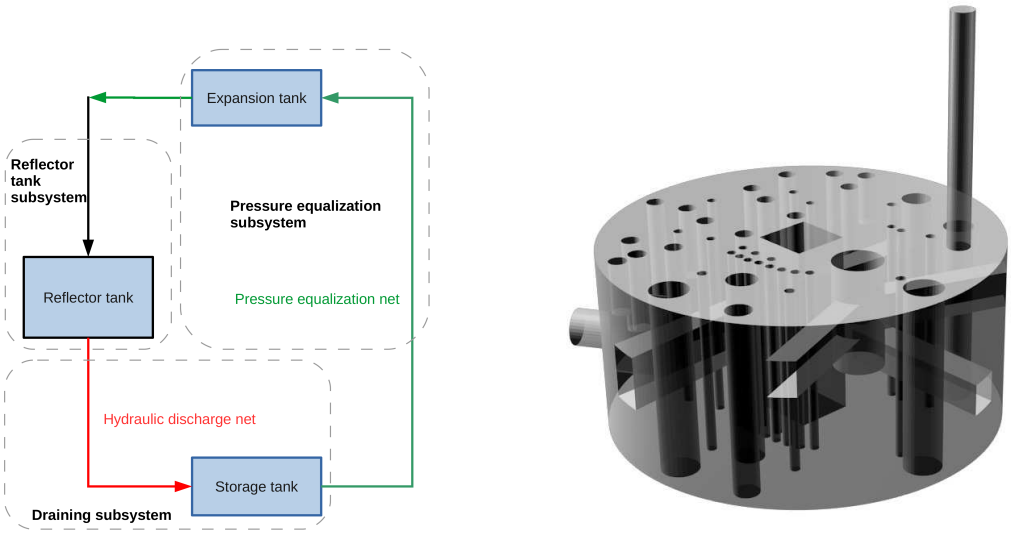

Figure 1: (Left) Diagram of the RA-10 SSS which is composed by three subsystems. (Black) Reflector tank subsystem. (Red) Discharge hydraulic net subsystem. (Green) Pressure equalization line subsystem. The arrows indicates the direction of the flow. (Right) Reflector tank of RA-10 SSS Mockup.

condition on top of the reflector tank due to the cover gas flow between the storage tank and the expansion tank.

In order to validate the 3D-0D multiscale model with experimental results we first solve the problem considering a Mockup configuration (Villarino and Doval (2011),INVAP (2013)). Afterwards, the validated model will be applied to the configuration of interest of RA-10 project, but results will not be presented in this article. The Mockup geometry is similar but larger than SSS for the RA-10 RR. Main features for both systems are listed in Table 1.

Characteristic	Mockup	RA-10
Tank height $[m]$	1.215	1.000
Tank radius $[m]$	1.300	1.000
Diameter of upper connection $[m]$	0.1524	0.1524
Diameter of discharge pipe $[m]$	0.2540	0.2647
Net volume $[m^3]$	5.558	2.492
Volume of internals $[m^3]$	1.041	0.649
Working fluid	Light water	Heavy water
Working cover gas	Air	He
Working pressure cover gas $[Pa]$	92000	121300

Table 1: Main characteristics of both cases: RA-10 SSS Mockup facility and RA-10 SSS.

3 MODEL FOR DRAINING AND PRESSURE EQUALIZATION SUBSYSTEM

3.1 Draining subsystem

A hydraulic discharge net attached to the reflector vessel conducts the draining liquid to a storage tank. This piping subsystem impose a pressure condition given by $p_{coupling}(t)$ over the outflow of the subsystem of the reflector tank. The piping subsystem is composed by a main duct (MD) with an internal diameter D_{MD}, several concentrated pressure losses represented by $\sum K_i^{MD}$, a manifold of six branches $\sum K_i^V$ each of one has a length L_V which contain a spherical valve with an associated pipe of diameter D_V, and finally a sudden expansion to the storage tank. The hydraulic net has an effective height given by the difference in the locations of the inlet and the outflow of the net $z_{net} = (z_{\text{outlet}} - z_{\text{inlet}})$. A zero-dimensional analysis of the hydraulic net allows to estimate the pressure at discharge patch ($p_{coupling}(t)$) given by Eq.(1).

$$\begin{aligned} p_{coupling}(t) &= p_{out} + (z_{\text{outlet}} - z_{\text{inlet}})\rho_l g + \rho_l \frac{V_{\text{MD}}^2(t)}{2}\left[f_{MD}\frac{\sum(L_i^{MD})}{D_{\text{MD}}} + \sum K_i^{MD} - 1\right] + \dots \\ &\quad \cdots + \rho_l \frac{V_{\text{V}}^2(t)}{2}\left[f_V \frac{L_V}{D_V} + \sum K_i^V + 1\right] \end{aligned} \tag{1}$$

Here $p_{coupling}(t)$ is the pressure at the outlet of the tank, p_{out} is the pressure at the discharge of the net which is coincident with the working gas pressure, z_{outlet} is the height of the outlet of the net, z_{inlet} is the height of the inlet of the net, $\sum K_i^{MD}$ and $\sum K_i^V$ are the effective local hydraulic resistances along the main duct and at each valve's branch, f_{MD} and f_V are the Darcy friction factors at the main duct and at each branch of the valve's manifold respectively, D_{MD} and D_V are the diameters of the pipes of the main duct and at the branch, $\sum L_i^{MD}$ and L_V are the corresponding lengths of the pipes to calculate the distributed friction factors and $V_{\text{MD}}(t)$ and $V_{\text{V}}(t)$ are the average velocities of the flow at main duct and at valve's branch. The values for the reference net used along all the computations presented in this work are listed in Table 2.

Characteristic	Value Mockup
p_{out} [Pa]	92000
$\sum K_i^{MD}$ [1]	4.56
$\sum K_i^V$ [1]	0.68
$\sum L_i^{MD}$ [m]	8.50
L_V [m]	1.00
$(z_{\text{outlet}} - z_{\text{inlet}})$ [m]	-6.27
D_{MD} [m]	0.2540
D_V [m]	0.1016

Table 2: Main geometrical characteristics of the discharge hydraulic piping subsystem.

3.2 Pressure equalization subsystem

The upper part of the reflector tank is connected to the pressure equalization subsystem. The purpose of this line is to equalize the pressure between the upper part of the reflector tank and the storage tank (see Fig.1). In the Mockup case this subsystem is not present and the ambient pressure acts on top of the tank.

4 SIMPLIFIED MODEL FOR SSS

To get knowledge of how the full solution will looks like, a simple model of a draining tank without internal details is developed. The dynamics is ruled by the unsteady-state macroscopic mechanical energy balance (Bird et al. (2002), Rechiman et al. (2014b)).
To evaluate the influence of the draining net on the discharge dynamics, two extreme cases were considered: A) The simple model without the hydraulic net attached to the tank. B) The simple model coupled in a dynamic manner with the hydraulic discharge net subsystem.

4.1 Case A: Simple model without hydraulic net

Let $t_{draining}$ be the time to drain an initial liquid height h_0 contained in a cylindrical tank of radius R_{tank} with a circular orifice of radius $R_{discharge}$ located at a height $y_{discharge}$.
Following (Bird et al., 2002), the draining time for the tank without the hydraulic net attached to it is given by Eq.(2).

$$t_{draining} = -\sqrt{\frac{(N-2)h_0}{2g}} \int_0^1 \frac{d\eta}{\sqrt{\eta - \frac{2\eta^{(N-1)}}{N}}} \tag{2}$$

In Eq.(2) g is the gravity acceleration while N and η are defined by: $N = \frac{R_{tank}^4}{R_{discharge}^4}$ and $\eta = \frac{h}{h_0}$.
Eq.(2) allows to know the time evolution of free surface position $h(t)$ assuming an equal pressure acting on top of the tank and at the discharge hole. It is interesting to note in Eq.(2) that the discharge time is independent of the type of the liquid and it is only governed by geometrical aspects.

4.2 Case B: Simple model with hydraulic net

To get a better description of the real case, we have modified the previous model by assuming that a pressure p_{top} is acting on top of the tank, and that a pressure imposed by a hydraulic net is acting on the discharge orifice represented by $p_{coupling}(t)$. The latter case is expressed by Eq.(3).

$$h(t)\frac{d^2h(t)}{dt^2} + \frac{1}{2}\left[1 - \left(\frac{R_{tank}}{R_{discharge}}\right)^4\right]\left(\frac{dh(t)}{dt}\right)^2 + g(y_{discharge} + h(t)) = \frac{(p_{coupling}(t) - p_{top})}{\rho_l} \tag{3}$$

In Eq.(3) the $p_{coupling}(t)$ is given by Eq.(1).

5 RESULTS OF THE SIMPLE MODEL APPLIED TO THE MOCKUP CASE

In Fig.(2) the solution for the remaining liquid inside the cylindrical tank for the simple model of the RA-10 SSS Mockup is shown. The dynamics is expressed by Eq.(2). The solution for the case considering an attached hydraulic net to it is also presented. The dynamics is represented by Eq.(3). It can be seen that the presence of the hydraulic discharge net cause an acceleration of the draining process. The mass flow for the base case (case A) could be up to 38% lower than the one for the case with the hydraulic net (case B) during the time of interest (Fig.(3)).
Possible uncertainties in the main parameters involved in $p_{coupling}(t)$ are analyzed. The following variations were considered: $\sum K_i^{MD} = [3.87; 5.24]$, $\sum L_i^{MD} = [4; 16]m$, $\Delta z = z_{outlet} - z_{inlet} = [-6.86; -5.69]m$, $\epsilon = [46\mu m; 1mm]$. The discrepancy in the solutions for

the position of the free surface according to the simple model are shown in Fig.(2) in a gray region. In Fig.(3) the discrepancy expressed in terms of the mass flow through the discharge of the system is also displayed.
It can be clearly seen from these results that the largest effect is in the case of 30% uncertainty in the concentrated hydraulic resistances. This may cause a variation up to 10% around the mass flow value of the base case (Fig.(2A) and Fig.(3A)). The second larger effect on the behavior of the system is the uncertainty on the height of the discharge net. In this case a variation up to 10% was taking into account (Fig.(2C) and Fig.(3C)). On the other hand, due to the relative small dimensions of the net, the distributed pressure losses present a negligible impact. Regarding this point, a wide variation of the total length of the main pipe and a wide variation of the roughness factor were considered. From Fig.(2B,D) and Fig.(3B,D) it can be seen that these two parameters present no major effects on the global dynamics (Fig.(2D) and Fig.(3D)).
The velocity of the descending free surface was computed and is shown in Fig.(4). It can be seen during the time of interest, that the presence of the net cause a nearly constant velocity for the drop of the liquid height in contrast with the case without it. The base model (case A) predicts a slower discharge than the one with the net (case B). This is due to the fact that the liquid column remaining within the tank of the simple case cause a lower driving force than the one with the net, which net effect is to enlarge the effective liquid column.

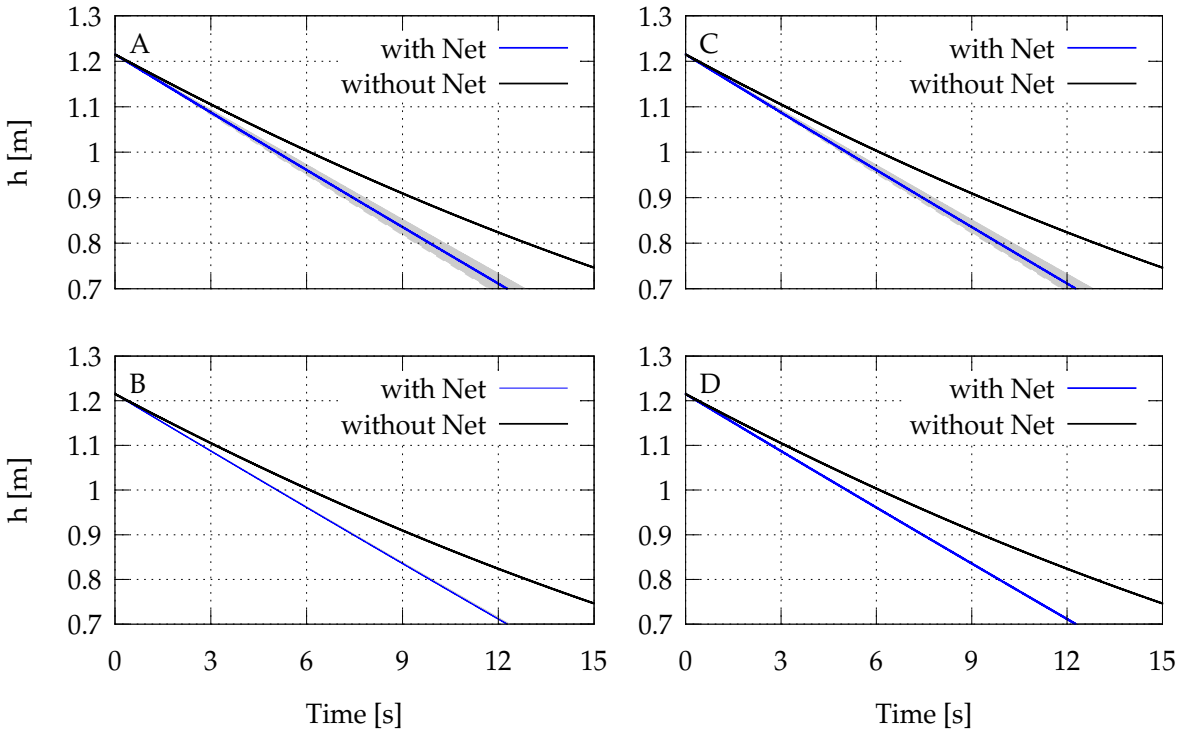

Figure 2: Remaining liquid height inside a tank for the case of the simple model given by Eq.(2) applied to the RA-10 SSS Mockup facility (black) and a the same tank with a discharge hydraulic net attached to it given by Eq.(3) (blue). The four cases show the range of variation of the solution taking into account variations on different parameters involved in $p_{coupling}$. (A) Influence of 30% uncertainty in the value of $\sum K_i^{MD} = [3.87; 5.24]$. (B) Influence in the value of the total pipe length considering the length of the main duct between $\sum L_i^{MD} = [4; 16]m$. (C) Influence of the net height of the hydraulic system up to 10% $\Delta z = z_{outlet} - z_{inlet} = [-6.86; -5.69]m$. (D) Influence of the pipe roughness $\epsilon = [46\mu m; 1mm]$. A wider variation of the solution is observed for cases (A) and (C), while negligible variation on the solution is observed for cases (B) and (C).

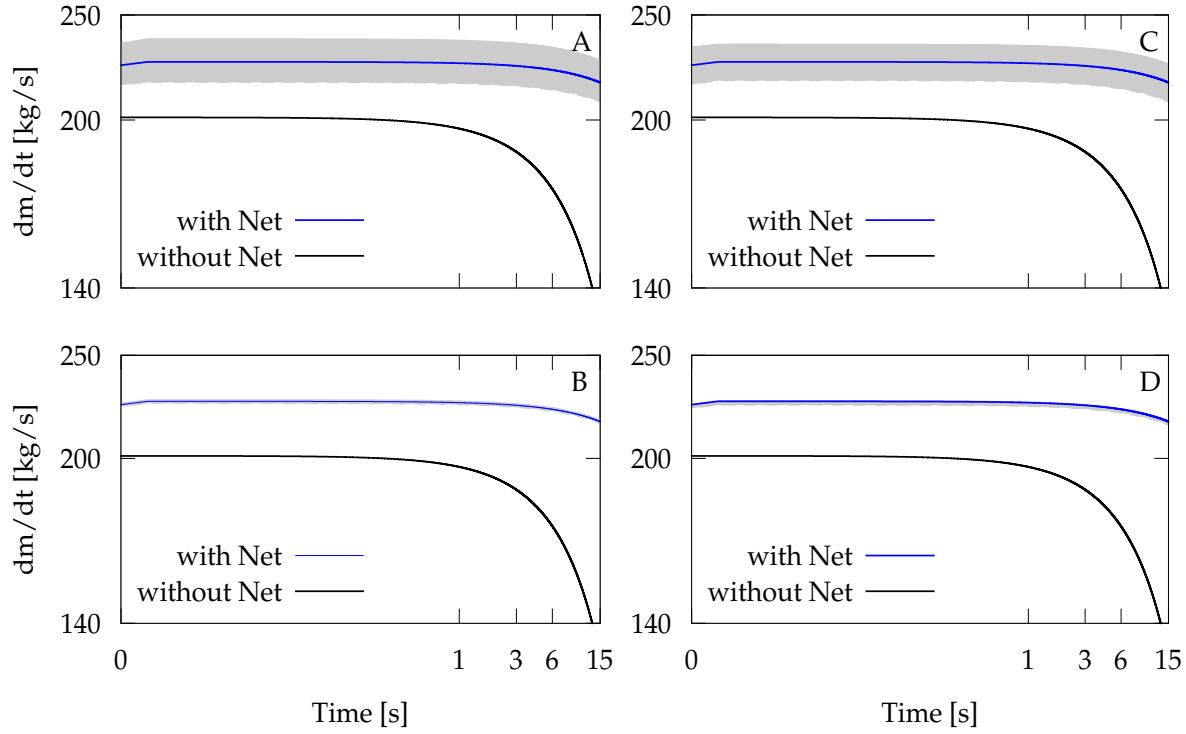

Figure 3: Time evolution of mass flow for the case of the simple model given by Eq.(2) applied to the RA-10 SSS Mockup facility (black) and a the same tank with a discharge hydraulic net attached to it given by Eq.(3) (blue). The four cases show the range of variation of the solution taking into account variations on different parameters involved in $p_{coupling}$. (A) Influence of 30% uncertainty in the value of $\sum K_i^{MD} = [3.87; 5.24]$. (B) Influence in the value of the total pipe length considering the length of the main duct between $\sum L_i^{MD} = [4; 16]m$. (C) Influence of the net height of the hydraulic system up to 10% $\Delta z = z_{outlet} - z_{inlet} = [-6.86; -5.69]m$. (D) Influence of the pipe roughness $\epsilon = [46\mu m; 1mm]$. A wider variation of the solution is observed for cases (A) and (C), while negligible variation on the solution is observed for cases (B) and (C).

6 COMPLETE MULTISCALE MODEL FOR SSS MOCKUP

6.1 3D model of reflector tank

In order to describe the particular two phase flow that takes place within the reflector tank, existing implementations of OpenFOAM(R) libraries version 2.2.2 were used. In particular, the incompressible, isothermal, multiphase solver *interFoam* was employed (Greenshields (2013a),Greenshields (2013b),OpenFOAM (2016),Marquez Damián (2013)).
Let t, $\mathbf{U}$, α, p and $\mathbf{f}$ be the time, the fluid velocity, the indicator function, the pressure and body forces respectively. The system of coupled partial differential equations composed by the mass conservation, the momentum equation and the transport of an indicator function may describe the problem of interest. The last is expressed by the system of Eq.(4) taking into account Newtonian fluids.

$$\begin{cases} \nabla \cdot \mathbf{U} = 0 \\ \frac{\partial \rho \mathbf{U}}{\partial t} + \nabla \cdot (\rho \mathbf{U}\mathbf{U}) = -\nabla p + \nabla \cdot (\mu \nabla \mathbf{U}) + (\nabla \mathbf{U}) \cdot \nabla \mu + \mathbf{f} \\ \frac{\partial \alpha}{\partial t} + \nabla \cdot (\alpha \mathbf{U}) + \nabla \cdot (\alpha(1-\alpha)(\mathbf{U}_L - \mathbf{U}_G)) = 0 \end{cases}$$

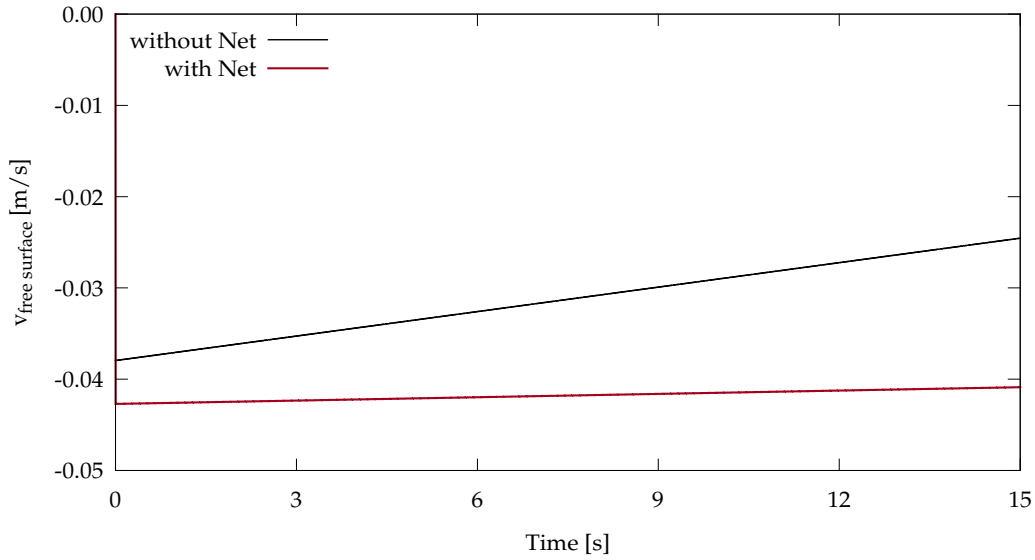

Figure 4: Velocity of the descending free surface predicted by the simple model applied to the draining tank of the RA-10 SSS Mockup geometry with and without the discharge net.

(4)

The interFoam solver use an Interface-Capturing Method approach based on the Volume of Fluid (VOF) technique (Hirt and Nichols, 1981). By employing this method, a single effective fluid is considered and the properties are determined by a weighted averaging with the indicator function:

$$\begin{aligned} \rho &= \alpha\rho_L + (1-\alpha)\rho_G \\ \mu &= \alpha\mu_L + (1-\alpha)\mu_G \\ \mathbf{U} &= \alpha\mathbf{U}_L + (1-\alpha)\mathbf{U}_G \end{aligned}$$

here ρ and μ are the density and dynamic viscosity where subscript L and G denote the liquid and gas phase respectively.

6.1.1 Turbulent flow model within the tank

The discrepancy in the solution if a turbulent model is added to the system of Eq.(4) is evaluated. Two cases were considered. In first place, a case in which only the fluid kinematic viscosity is used in the term associated to the viscous forces. On the other hand, a model which allows to calculate the Reynolds stress term $-\overline{U_i' U_j'}$ involved in the momentum equation expressed in terms of the Unsteady Reynolds Averaged Equation (URANSE). In particular, the κ-ϵ Realizable model was used (Pope (2000), Launder and Spalding (1974), Shih et al. (1995)). Therefore, two equations to solve the turbulent kinetic energy κ and its rate of dissipation ϵ to close the turbulent problem are added to the system of Eq.(4). These equations are coupled through the turbulent kinematic viscosity.

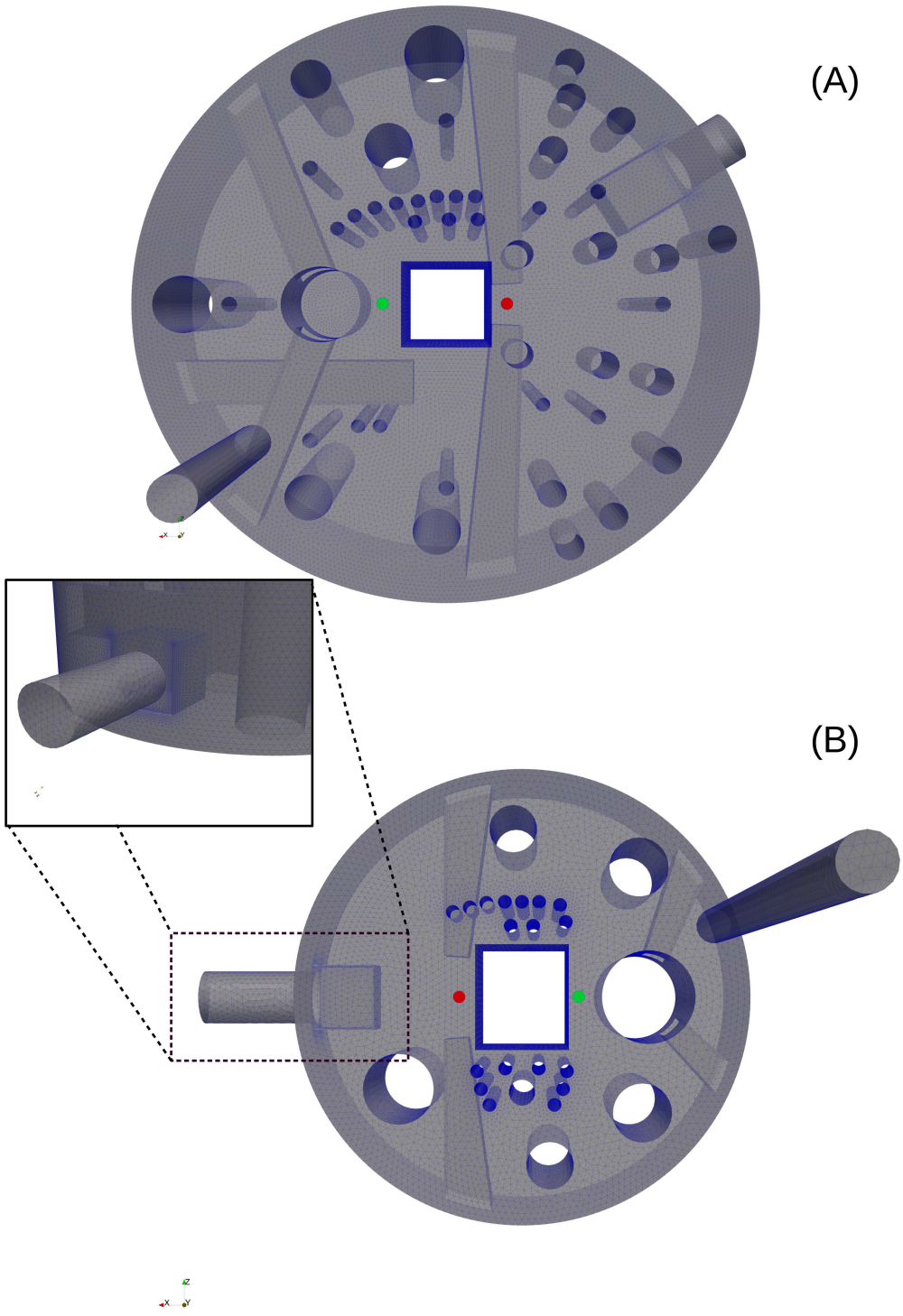

Figure 5: (A) Unstructured mesh of tetrahedrons of the RA-10 SSS Mockup tank. Surface mesh is shown. (B) Unstructured mesh of tetrahedrons for the geometrical configuration of interest of RA-10 SSS. Surface mesh is shown. (Inset) Detail of the discharge outlet of reflector tank. (Green dots) Location of the virtual rule (I). (Red dots) Location of the virtual rule (II).

6.2 Spatial discretisation of the problem

The spatial discretisation of the problem was made by using a non-structured mesh of tetrahedrons. The simulation domain for the 3D subsystem can be seen in Fig.(5).
The surface and volumetric meshes were generated by using NETGEN under Salome version 7.2.0 (OPEN CASCADE, 2013). In this work the Salome tool was used due to the fact that it allows to handle in a quite efficient manner the Boolean operations between bodies.
The NETGEN method allows to obtain a suitable mesh without slivers, which are badly distorted elements which render the mesh unsuitable for calculations (Dari and Buscaglia (1994),Rechiman et al. (2014a)).
For the RA-10 SSS Mockup case a reference mesh for the calculations was used. Main features are listed in Table 3. Computations on a refined mesh to evaluate possible discrepancies on the main global variables that rule the problem were also carried out.

Mesh Characteristic	Reference mesh Mockup	Fine mesh Mockup
N tetrahedrons	1447277	3931189
Faces	3025881	7993705
Internal faces	2763227	7731051
Volume $[m^3]$	5.558	5.558
Max. aspect ratio	7.95	6.68
Min. vol. $[m^3]$	6.09×10^{-9}	6.12×10^{-9}
Max. vol. $[m^3]$	3.48×10^{-5}	1.12×10^{-5}
Non-orth max. angle $[^o]$	67.87	67.79
Max. skewness	0.81	0.77

Table 3: Main properties of meshes.

6.3 Boundary Conditions for the 3D model of the reflector tank

The simulation domain is bounded by three main kind of patches: a discharge patch, the gas connection patch and the rest of the walls.
The boundary conditions (BC) applied on each *physical surface* are summed up in Table 4. The system of Eq.(4) is rewritten in terms of a field defined by $p_{rgh} = p - \rho\vec{g} \cdot \vec{x}$, where p is the pressure, $\vec{g}$ is the gravity acceleration and $\vec{x}$ denotes the coordinates of the point of interest. By using the p_{rgh} field, the formulation of the boundary condition is simplified.
For the discharge patch the *groovyTotalPressure* BC was used. This BC is part of a set of libraries developed by (Gschaider, 2013) and is similar than the *totalPressure* BC. The implementation of this BC has an additional feature that relies on program an expression for the reference pressure p_0. In the present problem, the pressure p_0 is determined by the coupling with the hydraulic net and it is equal to $p_0(t) = p_{coupling}(t) - \rho\vec{g} \cdot \vec{x}$.

Physical surface	BC $\mathbf{U}$	BC p_{rgh}	BC α
Discharge patch	zeroGradient	groovyTotalPressure	zeroGradient
Gas Connection patch	pressureInletOutletVelocity	totalPressure	inletOutlet
Walls	slip	buoyantPressure	zeroGradient

Table 4: Boundary condition applied on each *physical surface*.

6.4 Parallel calculations

The computations were carried out in a cluster of workstations connected by a Gigabit Ethernet line. Each node is an Intel(R) Core(TM) i7-3820 CPU 3.60GHz.

To make the domain decomposition (DD), the graph partitioning method based on the Scotch algorithm (Pellegrini, 2009) was used. This method splits the domain in a certain manner in order to minimize the amount of communications. In particular, it splits the domain in an approximately equal amount of cells per processor in order to keep the load balance. Furthermore, the main advantage of the Scotch method is the fact that the decomposition is the result of an optimization process in which the number of cells that are shared between two processors is as low as possible.
A performance analysis of the computing time with the available facilities, indicates that by using 28 processors on 7 nodes and applying the Scotch method to carry out the DD, is the optimum option for the problem at hand (Rechiman et al., 2014a).

7 MULTISCALE MODEL VALIDATION AND APPRAISAL OF THE MODELING

The multiscale numerical model was used to study two cases:

1. Case I: System of Eq.(4) using the two equation model $\kappa - \varepsilon$ Realizable to compute the turbulent kinematic viscosity.

2. Case II: System of Eq.(4) without using any model to compute the turbulent kinematic viscosity.

These two numerical experiments allow to quantify the unevenness in the solution between a complex model (Case I) and a self-effacing model (Case II).

7.1 Description of events in the RA-10 SSS Mockup

The initial state of the system is shown in Fig.(6), in which the reflector tank is full of liquid as well as part of the gas connection line. When the time evolution of the system starts, the liquid contained in the gas connection line, which height in the present model is 1.5 m, fully drains in approximately ~ 0.35 seconds. After the plug fall down, a violent liquid jet with a mean velocity of $7.3\frac{m}{s}$ and a maximum velocity of $11\frac{m}{s}$, impact over one of the cold neutron beams and a bowl-shaped crater is created, which depth is nearly 0.45 m at time 0.50 seconds.
From this time, a wave start to travel towards the direction where is located the discharge pipe. Diffraction and reflection patterns are generated while the wave interact with the tank internals, and the subsequent waves can reach 23 cm of amplitude. The first wave reaches the opposite side at 3 seconds of time evolution and reflects. After this time the waves start to diminish their amplitude until the free surface of the liquid is nearly smooth with minor distortions.
Ten seconds after the system start to evolve, a gas vain is established at discharge duct. We considered that when the average of the indicator function at discharge patch is below 0.5, the hydraulic net plays no role anymore and decouples. When this happens the ambient pressure will be acting on this patch. Due to the sudden change in the average of the indicator function at discharge patch, we choose as a criterion for decoupling the midpoint of the transition. When the gas vain is formed, the effective liquid cross section diminish up to 35% and is located as a horizontal half moon on the bottom of the pipe. Moreover, from now on the discharge dynamic get slower, the mass flow drops nearly 70% and a change in the slope of the draining curve is observed.

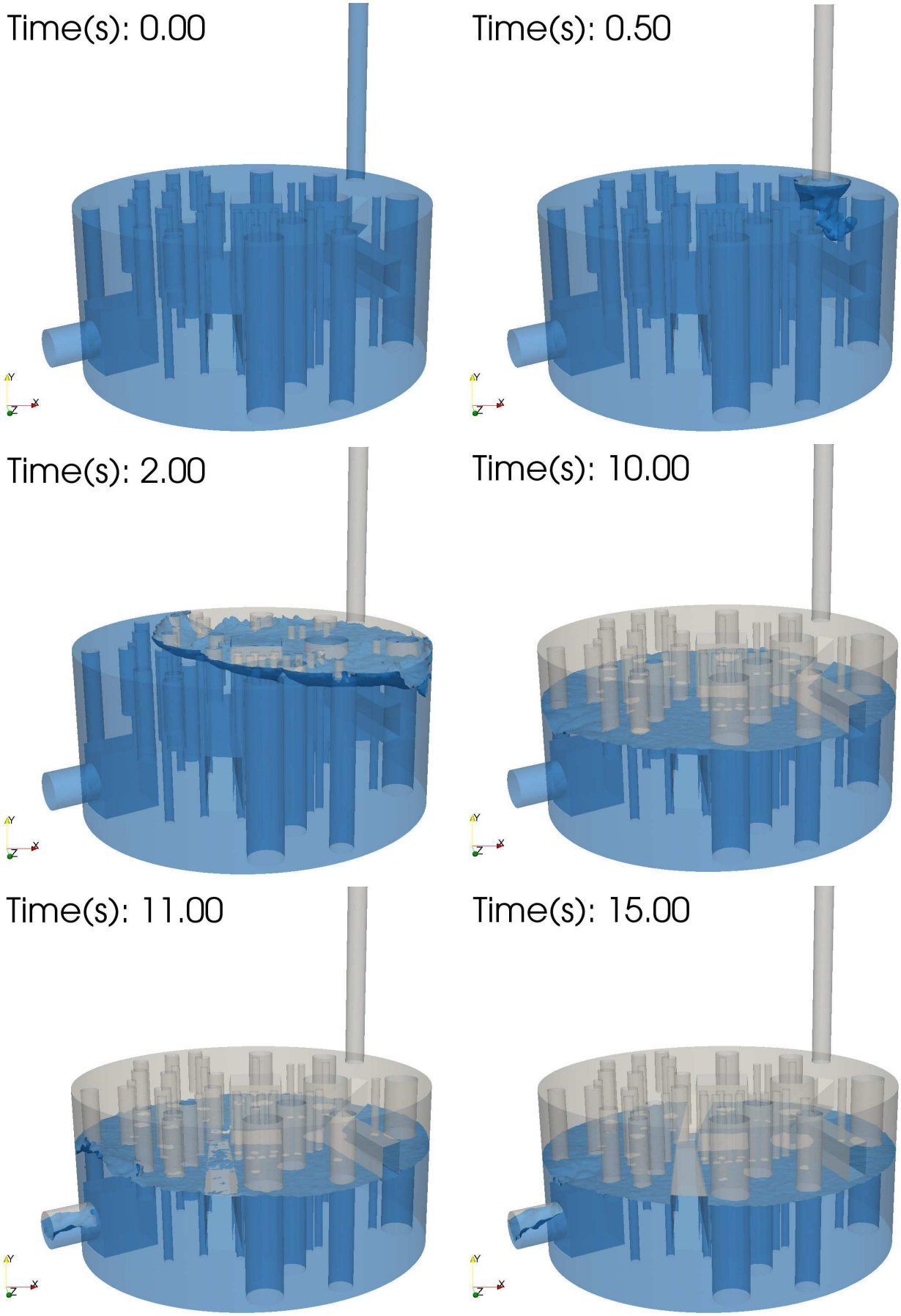

Figure 6: Time evolution sequence of the free surface inside the reflector tank predicted by the coupled model applied to the RA-10 SSS Mockup.

7.2 Quantification of effects involved in the RA-10 SSS Mockup

One of the main macroscopic variables of interest is the mass flux at discharge pipe. In Fig.(7) the computed draining curves for the two cases are shown.
Both cases are in perfect accord during the acceleration part (first 0.5 seconds) when the plug flows from top into the reflector tank. Moreover, they describe in a similar manner the global behavior of the discharge process, although the inclusion of the turbulent effect produce a smoother evolution than the case without it. This may be caused by the fact that the turbulent kinematic viscosity could be up to $\nu_T = 0.025\frac{m^2}{s}$, which is four orders of magnitude larger than the laminar kinematic viscosity. Then, the larger kinematic viscosity may attenuate flow fluctuations in the region where the mass flow is computed. It can be seen that at $t \sim 10s$ the gas vain is formed in the discharge duct and the hydraulic net is decoupled.

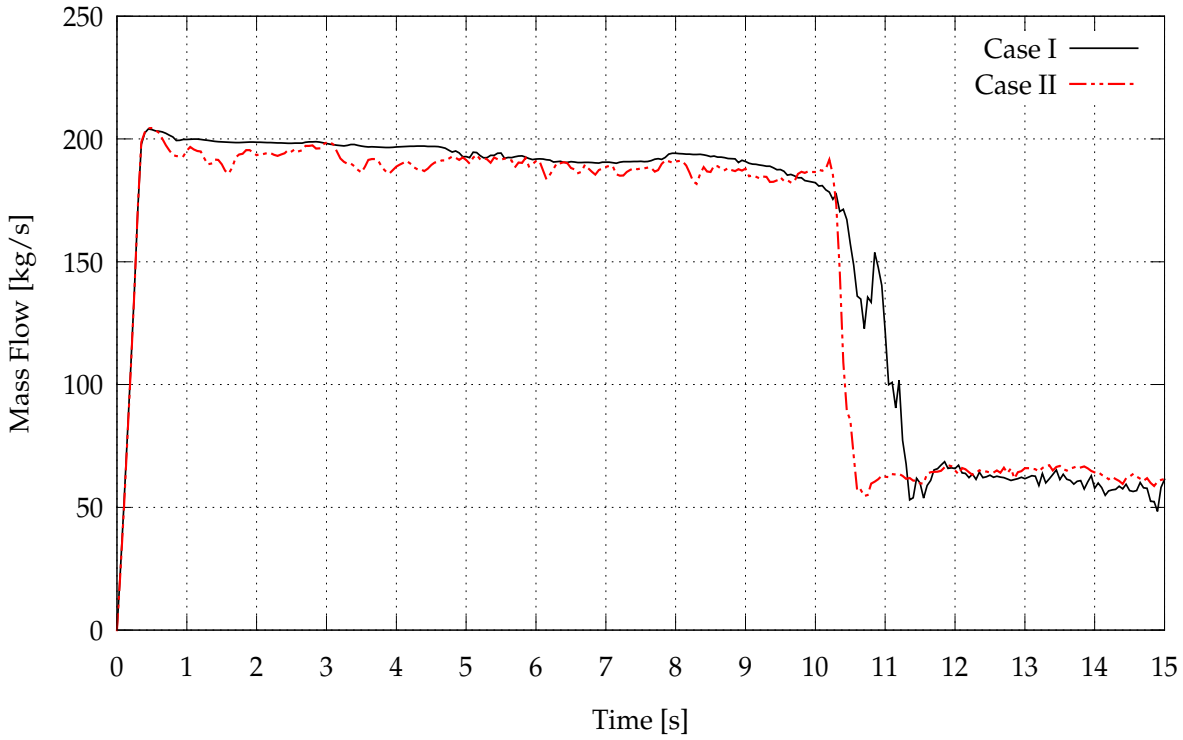

Figure 7: Mass flow of liquid phase at discharge patch for Cases (I) and (II) predicted by the coupled model applied to the RA-10 SSS Mockup geometry.

In Fig.(8) the contour for a fixed value $\alpha = 0.5$ of the indicator function is displayed. It can be seen a quite good agreement for the two cases except when the gas vain is established at discharge pipe. As a sake of completeness, although this *is not a surface dominated problem*, an additional simulation taken into account this effect was made. In Fig.(8) it can be seen that the Case (I) and (II) have a pretty good agreement with the mentioned additional simulation.
In order to evaluate the neutronic impact on the negative reactivity insertion caused by the removal of the reflector, the time evolution of the position of the free surface should be determined. This will be done in two ways: 1) in a *local manner* by calculating the interface position on virtual rules located near the reactor core. 2) in a *global manner* by calculating in an indirect way a mean effective position of the free surface by using the mass conservation law.
In Fig.(9) the time evolution of the free surface measured in a local manner as well as in a global manner for the numerical experiments associated with Case (I) and Case (II) are shown. The

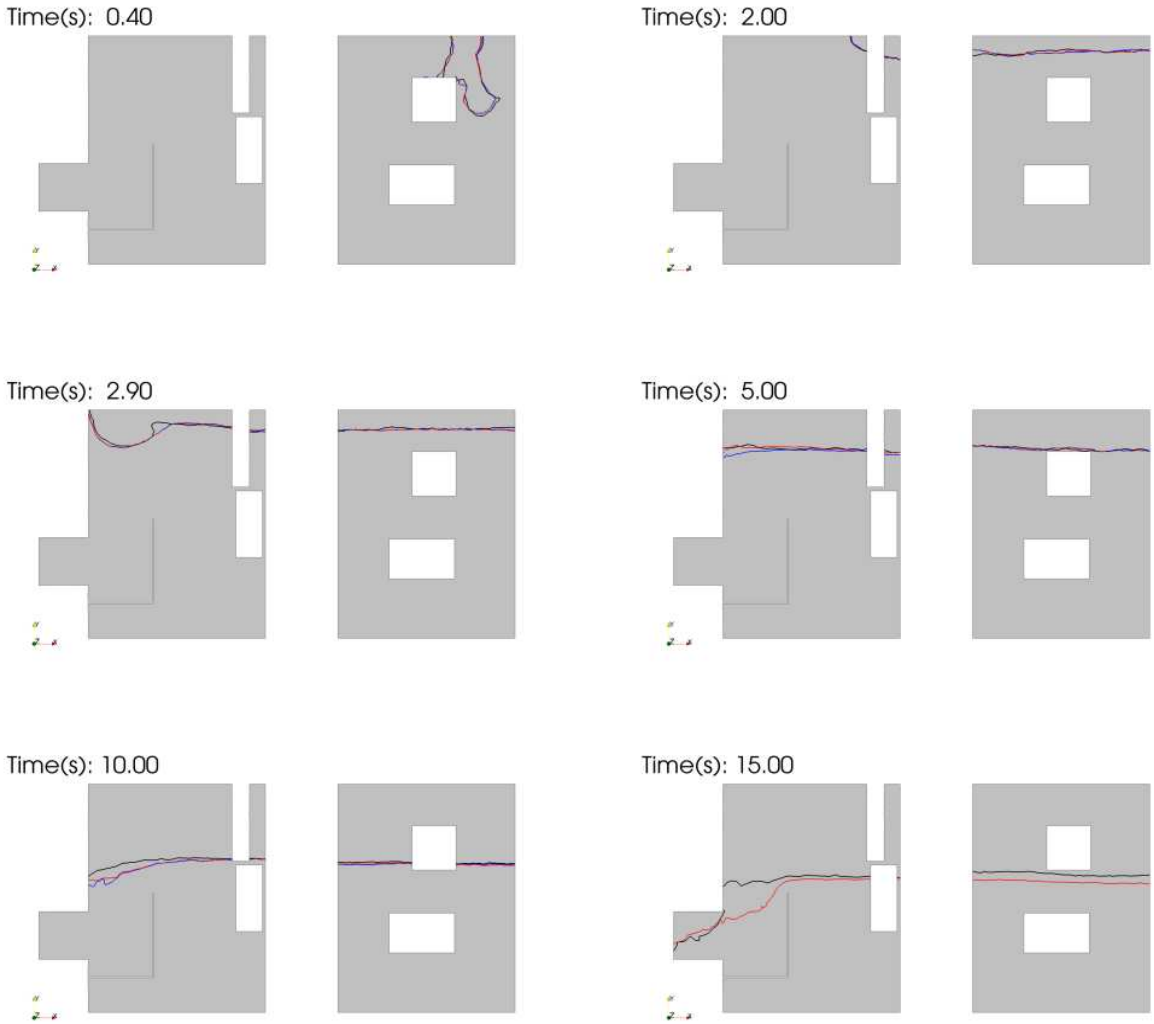

Figure 8: Time evolution sequence of the free surface predicted by the coupled model applied to the RA-10 SSS Mockup. (Red) Case I. (Black) Case II. (Blue) Additional simulation taking into account the surface tension effect.

global estimator for the liquid height remaining inside the tank is a decreasing linear monotonic function up to 10 seconds. At that time, a slope change occurs due to the fact that the lighter fluid starts to enter through the discharge pipe and then the hydraulic net is decoupled. Regarding the local estimators, it can be seen a delay of 1 second for virtual rule located at position (I) and 1.8 seconds for virtual rule located at position (II). The delay is attributed to the time the wave takes to reach these positions. For both cases, the local and global estimation for the location of the free surface are alike.

A comparison with previous experimental results reported in (INVAP (2013), Rechiman et al. (2015)) is also shown. It can be seen that the curves obtained with the present multiscale modeling behave in a similar manner than the experimental one. In particular, the numerical model correctly predicts tha last experimental point at the end of evolution. A mismatch is evident at early times. The discrepancy may be caused by two facts: in first place due to the nature of the experimental measurements, that is a local one. Secondly because of uncertainties in parameters involved in the hydraulic discharge net model.

All the previous different approaches to estimate the location of the free surface were compared with the simple model represented by Eq.(2) and Eq.(3). It can be clearly seen that the net

acts like a pump which accelerates the draining flow and in consequence the time required to emptying the same amount of liquid is faster than if the net would not been there. From Fig.(9) it can be seen that the prediction of the dynamics given by these two models enclosed all the cases formerly explained. Moreover, the results shows that the unsteady-state macroscopic mechanical energy balance approach with the net is a good predictor of the overall behavior of the system during the first 10 seconds of time evolution, even though no spatial distribution of the liquid reflector could be obtained. It is important to remark that when the air entrainment at discharge pipe occurs, this solution is no longer valid.
A key issue not addressed at the moment is the effect of the spatial discretization on the solution. A mesh convergence analysis is shown in Appendix A.

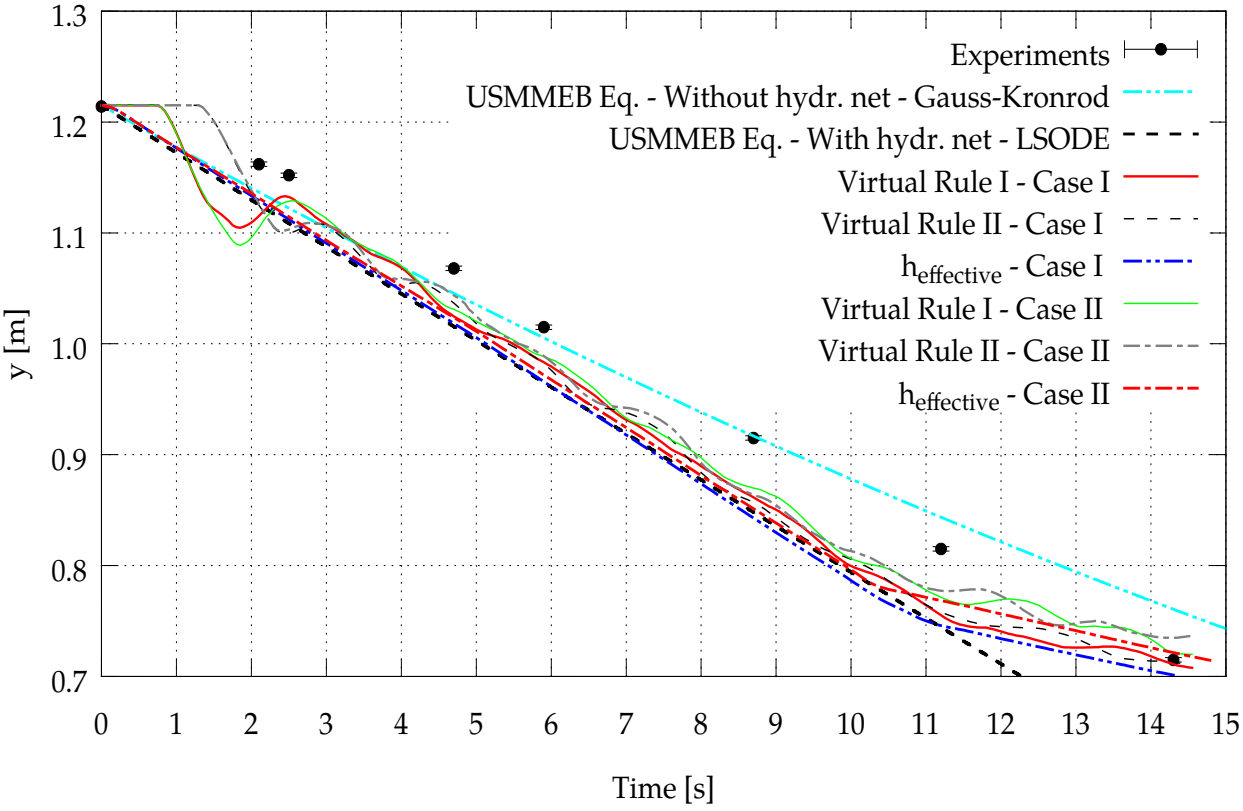

Figure 9: Draining curves of the RA-10 SSS Mockup. The position of the free surface was computed for the first 15 seconds of time evolution. The time $t = 0s$ corresponds to the moment in which the free surface cross the connection with the equalization line in the upper region of the reflector tank. (Black) Experimental measurements. (Cyan dotted line) Unsteady-state macroscopic mechanical energy balance (USMMEB) for a kindred model of the problem. Solution for Eq. (2) without the coupling with the hydraulic discharge net solved by a Gauss-Kronrod quadrature integrator. (Thick black dotted line) USMMEB given by Eq. (3) including the coupling with the hydraulic discharge net solved by a Livermore solver for ordinary differential equations (LSODE). (Solid red line) Local measurement of free surface position on a virtual rule located at position I for the Case I. (Thin dotted black line) Local measurement of free surface position on a virtual rule located at position II for the Case I. (Dotted blue line) Global estimation of free surface position for Case I. (Solid green line) Local measurement of free surface position on a virtual rule located at position I for the Case II. (Dotted gray line) Local measurement of free surface position on a virtual rule located at position II for the Case II. (Dotted red line) Global estimation of free surface position for Case II.

8 CONCLUSIONS

In the present work we have presented and discussed the results of a multiscale model applied to the RA-10 SSS Mockup geometry.
The main objective in this paper was to validate the multiscale methodology by comparing our results with theoretical and experimental data available for the RA-10 SSS Mockup configuration. We have implemented a robust model using OpenFOAM(R) suite which allows to make massive three-dimensional simulations with the current available facilities in order to contribute to a design stage of the SSS. It was proved that the multiscale approach of the complete system can accurately reproduce the overall behavior regarding the draining dynamics of the reflector tank. We have computed the free surface location by using local and global estimators. Both approaches indicate similar results and good agreement exists with experimental data measured in a local manner.
Although a simple model based on the unsteady-state macroscopic mechanical energy balance with an attached hydraulic net seems to be a good predictor of macroscopic values such as the discharge mass and a mean location of the free surface, the three-dimensional description is necessary to predict the decoupling moment of discharge net.

ACKNOWLEDGMENTS

The authors acknowledge support from RA-10 project and CNEA. We thanks to CIMEC from Universidad Nacional del Litoral for their support when endeavoring the first steps with OpenFOAM. We would also like to thank all the contributors in CFD online and OpenFOAM community.

REFERENCES

Bird R., Stewart W., and Lightfoot E. "Transport Phenomena", volume 2nd Edition. John Wiley & Sons, 2002.

Blaumann H., Vertullo A., Sánchez F., F.Brollo, and Longhino J. *"RA-10: A new argentinian multipurpose research reactor.". IAEA.*, 2013.

Dari E. and Buscaglia G. *"Mesh optimization: how to obtain good unstructured 3D finite element meshes with not-so-good mesh generators". Structural Optimization*, 8:181–188, 1994.

Greenshields C.J. " User Guide", volume version 2.2.2. CFD Direct Ltd., 2013a.

Greenshields C.J. "Programmers Guide", volume version 2.2.2. CFD Direct Ltd., 2013b.

Gschaider B.F. "Swak4Foam reference". Manual, 2013.

Hirt C. and Nichols B. *"Volume of Fluid (VOF) Method for the Dynamics of Free Boundaries".* 39:201–225, 1981.

INVAP. *"Segundo sistema de parada - validación del CFD para drenaje del tanque reflector". http://www.invap.com.ar*, 2013.

Launder B. and Spalding D. The numerical computation of turbulent flows. *Computer methods in applied mechanics and engineering*, 3(2):269–289, 1974.

Marquez Damián S. "An Extended Mixture Model for the Simultaneous Treatment of Short and Long Scale Interfaces". Ph.D. thesis, Universidad Nacional del Litoral, 2013.

OPEN CASCADE S. "The Open Source Integration Platform for Numerical Simulation., Salome tutorial. User's guide". SALOME, 2013.

OpenFOAM. "http://www.openfoam.org/". 2016.

Pellegrini F. "Contributions au partitionnement de graphes paralléle multi-niveaux". Ph.D. thesis, Université de Bordeaux I, 2009.

Pope S. "Turbulent flows". Cambridge University Press, 2000.

Rechiman L., Cantero M., and Dari E.A. *"Multiscale model of the Mockup of second shutdown system of RA-10 reactor.". Technical report RA-10 project, IN-ATN40MC-02/2015.*, 2015.

Rechiman L.M., Cantero M.I., and Dari E.A. *"Contributions of CFD to the analysis of the second shutdown system of the RA-10 research reactor.". International Group On Research Reactors IGORR Conference 2014*, 2014a.

Rechiman L.M., Cantero M.I., and Dari E.A. *"Hydrodynamic transient assessment of a draining tank". Mecánica Computacional Vol XXXIII. (2014)*, 2014b.

Shih T., Liou W., Shabbir A., Yang Z., and Zhu J. *"A new $\kappa - \epsilon$ eddy viscosity model for high Reynolds number turbulent flows". Computers Fluids*, 3:227–238, 1995.

Villarino E. and Doval A. *"INVAP's Research Reactor Designs.". Science and Technology of Nuclear Installations.*, page 490391, 2011.

APPENDIX A: SPATIAL RESOLUTION EFFECT IN THE RA-10 SSS MOCKUP CASE

In order to evaluate if the mesh resolution used for the calculations is good enough, the Case (II) was computed with a refined mesh. The refined mesh is composed by 728283 points and 3931189 tetrahedrons. The general characteristics of this mesh are listed in Table 3.

In Fig.(10), the drained mass flow calculated with the reference mesh and with the refined mesh are shown. It can be seen that a good agreement exists between them. Moreover, the integral of the mass flow along the 15 seconds of time evolution for both cases was estimated. The discharged mass of liquid computed with the reference mesh is $m = 2234.41$ kg. On the other hand, the discharged mass of liquid calculated with the refined mesh is 2234.72 kg. Then the discrepancy in the solution of the mass leaving the tank is 0.02%. These results suggest that the solution is converged for the reference mesh used along the present work.

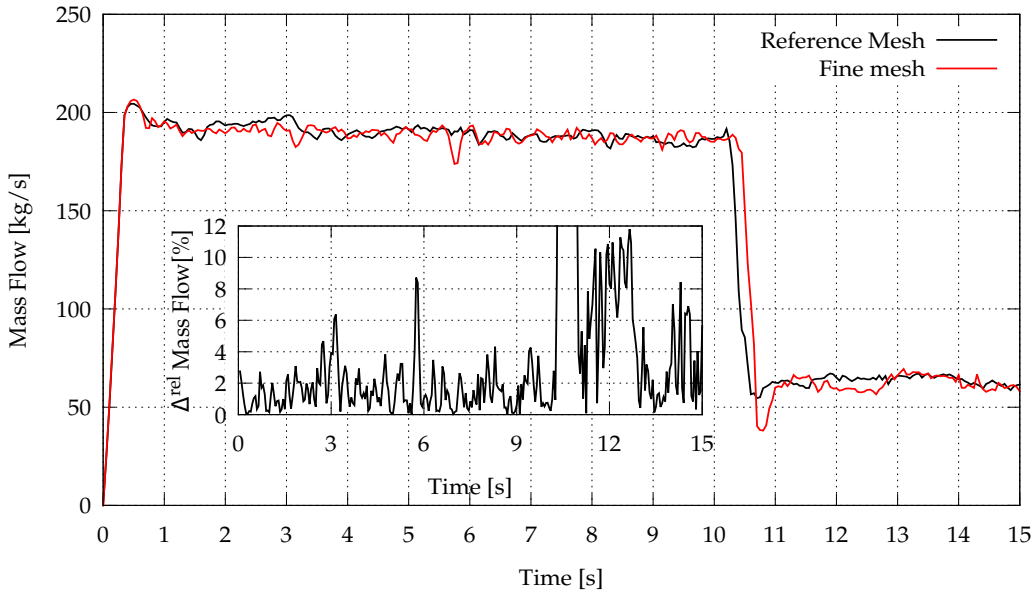

Figure 10: Mass flow of liquid phase at discharge patch with the configuration of Case II for RA-10 SSS Mockup. (Black) Reference mesh. (Red) Fine Mesh. (Inset) Relative difference between the solutions.